Journal of
Microscopy

Journal of Microscopy, Vol. 00, Issue 0 2014, pp. 1–11
Received 13 January 2014; accepted 31 July 2014

doi: 10.1111/jmi.12172

Tracking protein dynamics with photoconvertible Dendra2 on spinning disk confocal systems

ELENA WOODS*, JANE COURTNEY†, DIMITRI SCHOLZ‡, WILLIAM W. HALL* & VIRGINIE W. GAUTIER*

**Centre for Research in Infectious Diseases, School of Medicine and Biomedical Science, University College Dublin (UCD), Dublin, Ireland*

†Dublin Institute of Technology, Kevin St, Dublin, Ireland

‡UCD Conway Institute of Biomolecular & Biomedical Research, School of Medicine and Biomedical Science University College Dublin (UCD), Dublin, Ireland

Key words. Dendra2, live cell imaging, photoconversion, spinning disk confocal microscopy.

Summary

Understanding the dynamic properties of cellular proteins in live cells and in real time is essential to delineate their function. In this context, we introduce the Fluorescence Recovery After Photobleaching-Photoactivation unit (Andor) combined with the Nikon Eclipse Ti E Spinning Disk (Andor) confocal microscope as an advantageous and robust platform to exploit the properties of the Dendra2 photoconvertible fluorescent protein (Evrogen) and analyse protein subcellular trafficking in living cells. A major advantage of the spinning disk confocal is the rapid acquisition speed, enabling high temporal resolution of cellular processes. Furthermore, photoconversion and imaging are less invasive on the spinning disk confocal as the cell exposition to illumination power is reduced, thereby minimizing photobleaching and increasing cell viability. We have tested this commercially available platform using experimental settings adapted to track the migration of fast trafficking proteins such as UBC9, Fibrillarin and have successfully characterized their differential motion between subnuclear structures. We describe here step-by-step procedures, with emphasis on cellular imaging parameters, to successfully perform the dynamic imaging and photoconversion of Dendra2-fused proteins at high spatial and temporal resolutions necessary to characterize the trafficking pathways of proteins.

Introduction

The subcompartmentalization of eukaryotic cells into membranous and a-membranous organelles enables the separation of incompatible biochemical processes and facilitates the spatiotemporal regulation of cellular responses. Accordingly, subcellular protein transport controls protein functioning by regulating their access to relevant organelles (Scheer & Hock, 1999; Mayer & Grummt, 2005; Olson & Dundr, 2005; Hernandez-Verdun, 2006a,b; Muro *et al.*, 2010).

Photoconvertible fluorescent proteins represent powerful tools for the investigation of protein dynamics, enabling the tagging and real-time tracking of proteins and organelles in live cells. Unlike conventional fluorescent proteins, these proteins can either 'turn on' their fluorescence (photoactivation) or change their emission wavelength in response to photostimulation [photoconversion (PC)] with ultraviolet or intense blue light, a property which enables the optical highlighting of molecules of interest in the target area, and which can be exploited to provide high spatiotemporal resolution of dynamic cellular processes (Lukyanov *et al.*, 2005; Chudakov *et al.*, 2006; Chudakov *et al.*, 2007a). Dendra2 is a *Dendronephthya* sp. derived photoconvertible protein that undergoes irreversible conversion from a green to a red fluorescent state upon exposure to ultraviolet (405 nm) or high-intensity blue light (488nm; Chudakov *et al.*, 2007b; Adam *et al.*, 2009). Unlike other Kaede-like proteins (Kaede, Dronpa, mEOSfp), Dendra2 is a monomer which, in the dark, rapidly matures to the green fluorescent state with a half-time of 90 min at 37°C, making it particularly suited to the photolabelling of proteins at the single cell level (Gurskaya *et al.*, 2006). Preconversion, Dendra2 has excitation/emission maxima of 490/507 nm, allowing for excitation with low intensity blue light (488 nm laser line) and detection with a standard GFP filter set. PC of Dendra2 results in excitation/emission maxima at 553/573 nm and can be excited with either 543, 561 or 568 nm laser lines with emission detection using a standard RFP filter set (Chudakov *et al.*, 2007b).

Dendra2 has been widely used to provide insights into the trafficking of nuclear, structural and membrane proteins

Correspondence to: Virginie W. Gautier, Centre for Research in Infectious Diseases, School of Medicine and Biomedical Science, University College Dublin (UCD), Dublin, Ireland. Tel: +353-1-716-1229; e-mail: Virginie.Gautier@ucd.ie

in live cells. At present, there are two different platforms described for visualizing Dendra2, laser scanning confocal microscopes (LSCM) and wide-field fluorescence microscopes (Chudakov *et al.*, 2007b; Baker *et al.*, 2010; Kuzmenko *et al.*, 2011). LSCM is a popular imaging tool, which provides high spatial but limited temporal resolution of cellular processes. Techniques such as fluorescence recovery after photobleaching (FRAP) and more recently, photoconvertible proteins are routinely employed on LSCM platforms to study protein dynamics in live cells (Sprague & McNally, 2005; Mueller *et al.*, 2010). Typically, images are acquired by scanning a point of laser illumination in a raster-pattern across the sample, sequentially building a 2-D image by detecting each point's emission through a confocal pinhole (White *et al.*, 1987; Fldes-Papp *et al.*, 2003). In practice, this results in slow image acquisition that can hamper the temporal resolution of highly dynamic cellular processes (Nakano, 2002). Furthermore, high speed imaging on LSCM requires intense illumination of fluorescent samples to compensate for limited detector efficiency, resulting in photobleaching of fluorophores as well as significant cellular phototoxicity (Wang & Dunn, 2005). Together, these technical limitations may affect some applications of LSCM for dynamic live cell imaging. The Nipkow spinning disk confocal is an advanced imaging platform that 'multiplexes' image acquisition, simultaneously scanning multiple points in a sample and collecting fluorescence emission through multiple confocal pinholes. This innovation over conventional LSCM enables rapid image acquisition with minimal photobleaching and phototoxicity, making it the tool of choice for dynamic live cell imaging and revealing new insights into diverse physiological processes (Genka *et al.*, 1999; Inou & Inou, 2002; Tanaami *et al.*, 2002; Wang & Dunn, 2005; Nelson *et al.*, 2010; Jenne *et al.*, 2011; Enoki *et al.*, 2012; Samantha Stehbens *et al.*, 2012; Lam *et al.*, 2014). Until recently, technical limitations with spinning disk confocals have prevented their usage for bleaching applications, as these methods rely on precise subcellular targeting of regions for prolonged irradiation with the exciting laser. This issue was resolved with the advent of the FRAP-PA unit (Andor), a photobleaching module consisting of a dual galvanometer scan head which can be configured for both FRAP and PA (photoactivation) utilities, coupling the rapid live cell imaging capabilities of a spinning disk confocal with established methods to study protein dynamics.

We describe here a novel and robust procedure for employing the FRAP-PA module (Andor) for the PC of Dendra2 on a Nikon Eclipse Ti-E spinning disk confocal microscope (SDCM) (Nikon Instruments Europe B.V., Amsterdam, The Netherlands) driven by Andor IQ2.6 software. We demonstrate the practicability of our experimental set up in capturing and distinguishing rapid and differential subcellular protein dynamics using Dendra2Fibrillarin and Dendra2UBC9, two nuclear proteins with distinct localizations and trafficking characteristics.

Results and discussion

(1) Experimental set up for the PC and imaging of Dendra2 fusion proteins trafficking in live cells using SDCM (Fig. 1).

To establish a benchmark for performing live cell PC experiments on a SDCM based platform, we chose to visualize the trafficking of Dendra2 alone, together with UBC9 and Fibrillarin, fused to Dendra2. As opposed to Dendra2, which displays minimal interaction with its cellular environment and diffuses freely throughout the cell, UBC9 and Fibrillarin show selective interactions and preferential accumulation within the premyleocytic leukaemia (PML) bodies and the nucleolus, respectively (Phair RDM, 2000; Villagra *et al.*, 2006). Of note, Western blot analysis confirmed the expression of the fusion proteins with their expected molecular weight (Fig. S1). Twenty-four hours posttransfection, HeLa cells expressing Dendra2 fusion proteins were imaged at 37°C in a humidified atmosphere, on a Nikon Eclipse Ti E Spinning Disk microscope (Andor) equipped with a 100× 1.4 N.A. oil objective and 405 nm, 488 nm and 561 nm diode laser lines and customized with a FRAP-PA unit (Andor, Oxford Instruments Company, Belfast, N. Ireland) used for PC experiments. The FRAP-PA unit was configured 'in line' to the imaging path which enabled its sequential operation in bypass mode, where it functions as a relay optic and facilitates imaging through the confocal spinning disk unit, or FRAP-PA mode, where it acts as a laser scanner in order to execute PC. Of importance, the switching time between modes is optimized at 20 ms, in order to minimize the downtime between PC and imaging. An iXon 897 CCD camera (Andor) and Andor IQ2 acquisition software were employed to record the PC experiments. Our approach involves three main operations, which are described below and included in our step by step protocol.

Step by step PC protocol

The acquisition phase of PC protocol, as illustrated in Figure 1, includes the following steps:

(1) The desired focal plane (target cell) is located in the field of view using transmission light and a 100× 1.4 oil objective.
(2) Prior to PC, Dendra2 is imaged, within the target cell (field of view), in its native emission state in the green channel, using the 488 nm laser line (50 mW nominal output) in conjunction with a 'GFP' emission filter (512/18 nm; Table 1). Importantly, for imaging, the laser power was attenuated to 1–8.5% to avoid unspecific PC as described below (Table 1).
(3) A region of PC is delineated and classified as 'FRAP-PA'.
(4) A preconversion image is recorded in the red channel, using a 561 nm, 50 mW diode pumped solid stare laser (20–35%) for excitation in conjunction with an RFP emission filter (624/40 nm; Table 1), to ensure that no preconversion events had occurred.

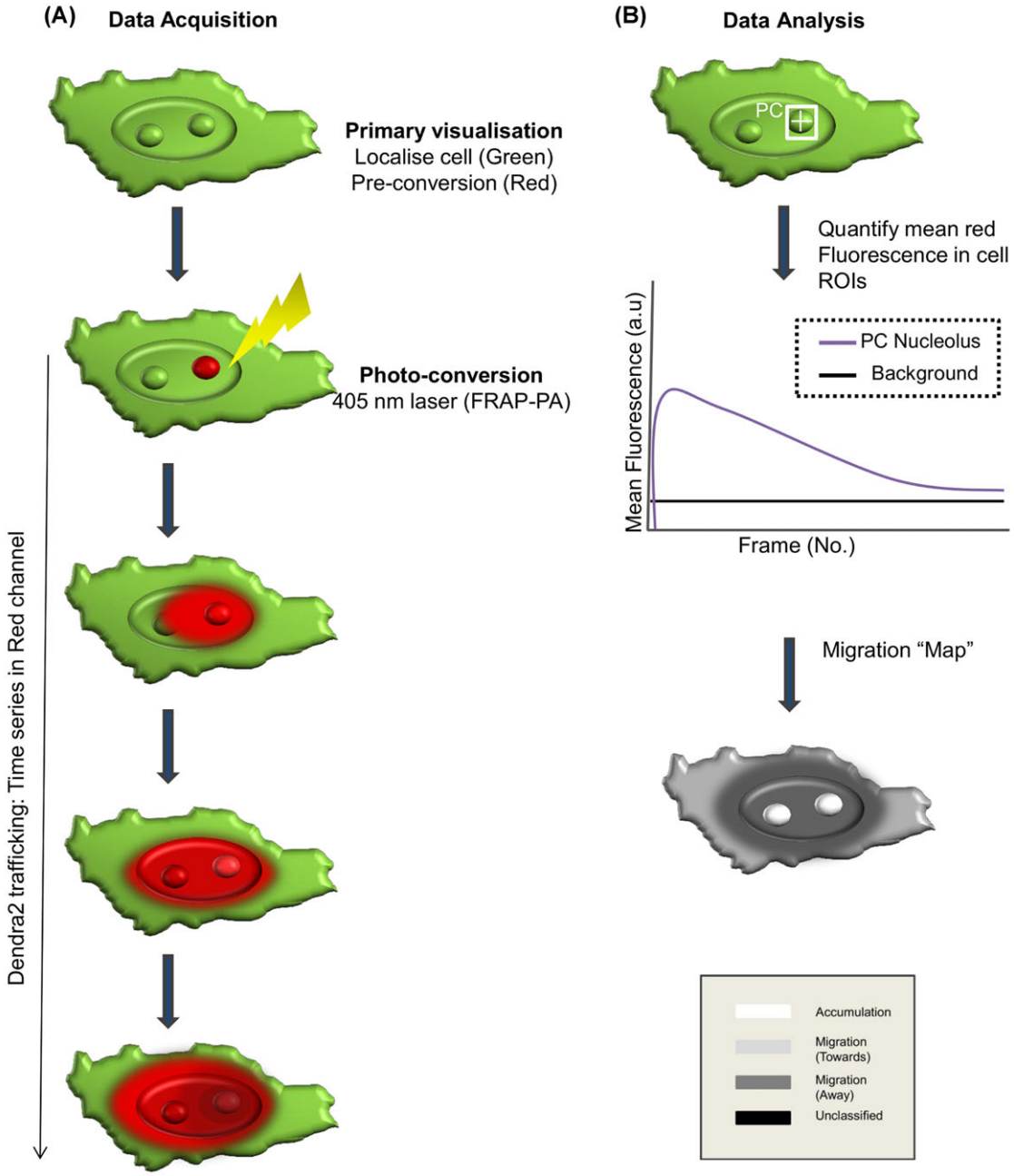

Fig. 1. Overview of photoconversion protocol. (A) Data Acquisition: 24 h posttransfection, HeLa cells expressing Dendra2 (Green) are imaged in the Green channel (Table 1) on a Nikon Eclipse Ti E Spinning Disk Microscope. Preconversion events are monitored by recording a preliminary image in the Red channel. Next, a subcellular region is targeted with the FRAP-PA unit and photoconverted using a 405 nm diode laser at 25% laser power for 1000 μs. In parallel, an image is recorded in the Green channel to confirm the target accuracy of the photoconverting laser. Subsequently, Dendra2 (Red) trafficking events are monitored through acquisition of a Time series in the Red channel using an iXon 897 EMCCD (Andor) camera (−70°) and Andor IQ2 acquisition software. (B) Data analysis: The data set is exported as a Multi-Tiff file and analysed using MATLAB. Subsequently, Dendra2 trafficking is characterized by analysing the variation in red mean fluorescence intensity within cellular regions of interest (ROIs) over the time series. Selection and demarcation of the ROIs depend on the protein of interest trafficking characteristics. Finally a 'migration map' is generated by classifying the signal variation (SD) of individual pixels over the time series, providing an overview of Dendra2 trafficking during the time series with respect to the point of photoconversion. The migration map is coded to represent different trafficking behaviours. White: Accumulation within a region. Dark Grey: migration away from the region of photoconversion. Light grey: migration into a region. Black: unclassified.

(5) Back to the green channel, the PC region is specifically irradiated using the 405 nm diode laser line of the FRAP-PA unit at 25% power for 1000 μs, and an image in the green channel is immediately recorded to visualize the loss of green signal due to the PC as described below.
(6) In the Red channel, single section images are recorded by time lapse imaging. To capture fast trafficking Dendra2 fusion proteins, images can be collected at the shortest possible acquisition speed using the acquisition parameters described in Table 1. Of note, After PC, a delay of 80 ms to the start of the time lapse is unavoidable due to the necessity of switching between the Green filter (for PC), and the Red filter (for time lapse acquisition).
(7) Dendra2 trafficking events are characterized using a MATLAB (Mathworks, ver. 7.1) based quantitative image analysis algorithm, MATtrack, by analysing the variation in mean red fluorescence intensity within distinct subcellular regions over the time series (as described below).

Optimal conditions to visualize Dendra2 in the green channel (Step 2)

The first critical step was to delineate the optimum imaging parameters for imaging Dendra2 in both green and red channels. Indeed, Dendra2 can be photoconverted with blue laser light (488 nm) of sufficient duration and intensity, potentially resulting in undesirable PC events occurring during preliminary localization of Dendra2 expressing cells. Hence, we titrated the 488 nm laser intensity level to a minimum value (1–8.5%) to image the green form of Dendra2 without triggering nonspecific PC or induce photobleaching (Table 1). Figure 2 provides an overview of the integrated average green or red fluorescence intensity of cells expressing Dendra2 before (Fig. 2A) and after (Fig. 2B) PC on the SDCM. Dendra2 fluorescence exhibited minimal bleaching after prolonged imaging on the SDCM (120 frames; Figs. 2A,B). Please note the absence of nonspecific PC (red fluorescence) during the time series on the SDCM (Fig. 2A). We further confirmed the efficacy of the SDCM for image acquisition of Dendra2 (Green) by comparing preconversion occurring during time series recorded on both the SDCM and an Olympus Fluoview FV1000 LSCM (Olympus Corporation, Tokyo, Japan) (Fig. 2C). Importantly, acquisition on the SDCM resulted in a substantial decrease in Dendra2 PC in comparison to the Olympus Fluoview FV1000, highlighting the utility of the SDCM for routine imaging of Dendra2.

Optimal conditions to perform Dendra2 PC (steps 3–6)

The next critical step was to configure the SDCM FRAP-PA unit to delineate the optimum Dendra2 PC parameters (intensity and pixel dwell time) using a 405 nm laser line. We determined that irradiation of a PC area with the 405 nm laser line necessitated 25% of its laser power for 1000 μs pixel^{-1} to photoconvert Dendra2, Dendra2Fibrillarin and Dendra2UBC9 (Figs. 3–5; Table 1).

Data analysis (Step 7)

Initial verifications included examining the raw data, using the Andor IQ2 acquisition software, to confirm the absence of unspecific PC or bleaching events. The data was then exported as a multitiff format (.tiff) and processed using MATtrack; a novel programme developed in MATLAB (Mathworks, ver. 7.1) and tailored to characterize the subcellular trafficking trends of photoconvertible proteins and their dominant flow of motion. Briefly, this program automates multiple image processing functions, including noise filtering, normalization of fluorescence intensity, temporal smoothing and the integrated average fluorescence intensity and SD. Next, the software analyses the mean fluorescence intensity in user-defined cellular regions of interest (ROI) over time. ROIs are identified by the user by selecting a point of interest and employing a seeded region growing algorithm to search for pixels of similar mean intensity in the surrounding area (up to 50 pixels; Adams & Bischof, 1994). Finally, MATtrack classifies the dataset based on the variation of the fluorescent signal of each individual pixel from the mean (i.e. SD) throughout the cell, over the time lapse. Next, it constructs a colour-coded image to map protein migration routes (Fig. 1). White: Accumulation within a region. Dark Grey: Migration away from the region of PC. Light grey: Migration into a cellular region. Black: Unclassified. This 'migration map' provides an overview of the protein intracellular flows during the time series with respect to the point of PC.

(2) Applications of our PC experimental set up using Dendra2, Dendra2UBC9 and Dendra2Fibrillarin.

We tested our experimental platform in distinct experimental settings to track the migration of fast trafficking proteins such as UBC9 and Fibrillarin. In the applications described below, PC experiments were performed with the Nikon SDCM customized with a FRAP-PA unit, using HeLa cells transiently transfected with corresponding constructs and with the imaging parameters described in Table 1.

Application 1: free diffusing Dendra2 protein

As an inert and non-binding protein, unconjugated Dendra2 provides a model for purely diffusive behaviour in a cellular environment. Indeed, we observed that Dendra2 signal diffusely localized in both nucleoplasmic and cytoplasmic subcompartments with some exclusion from prominent subnuclear organelles (nucleoli; Fig. 3A). Hence, we targeted a region of nucleoplasm for PC (white cross) and monitored adjacent ROIs for Dendra2 relocalization using the red channel (Table 1; Figs. 3A,D). These included a nucleolus

Table 1. Optimal imaging parameters for Dendra2 on the Nikon Eclipse Ti E spinning disk confocal.

Channel	Laser	Laser intensity (%)	Pixel dwell time (μs)	Confocal modality	Exposure time (ms)	Emission filter (nm)	Disk speed (RPM)
Green	488 nm	1–8.5	–	CSU	40	512/18	5000
Red	561 nm	20–35	–	CSU	50	624/40	5000
Photoconversion	405 nm	25	1000	FRAP-PA	N/A	N/A	–

adjacent to the photoconverted region plus additional regions in the nucleoplasm and cytoplasm. One second after PC, Dendra2 was detected in the nucleolus adjacent to the photoconverted region (ROI 1). Concomitantly, we observed a wave of Dendra2 migration throughout the nucleoplasm (ROI 2) with subsequent diffusion across the nuclear envelope and accumulation in the cytoplasm (ROI 3). Accumulation in the nucleolar region (ROI 1) was lower than in the nucleoplasm (ROI 2), suggesting that the capacity for protein accumulation in the nucleolus is diminished with respect to the nucleoplasm. The migration map highlights the free diffusion of Dendra2 in the nucleoplasmic and cytoplasmic compartments (Fig. 3B).

Application 2: investigating the subnuclear trafficking of Dendra2Fibrillarin

Dendra2Fibrillarin presented a diffuse signal in the nucleoplasm with higher fluorescence intensity in prominent spherical nuclear structures corresponding to nucleoli (Fig. 4A).

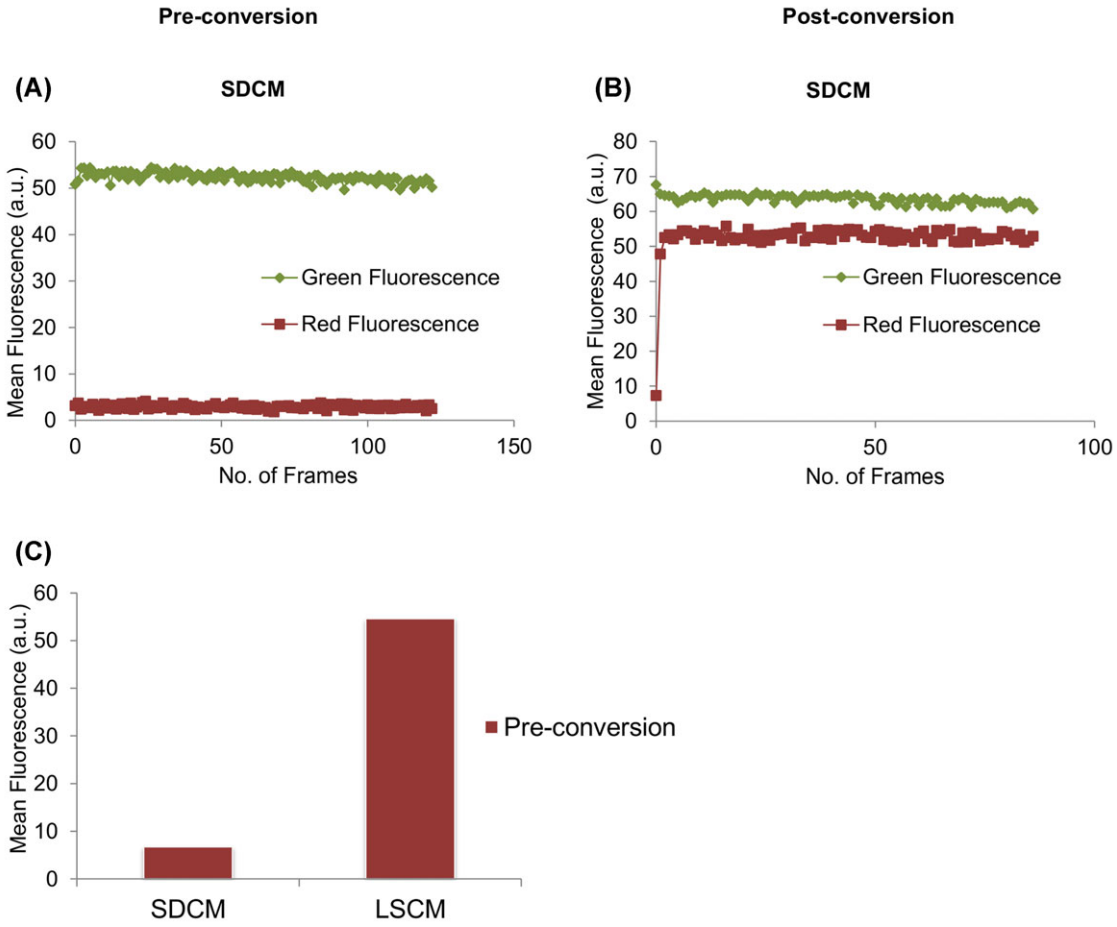

Fig. 2. Overview of Dendra2 photostability on an Andor revolution spinning disk confocal microscope. HeLa cells transiently expressing Dendra2 were imaged alternately in the Green and Red channels (one frame per 3 s), preconversion (120 frames) (A) or postconversion (86 frames) (B) on a Nikon Eclipse Ti E spinning disk microscope (SDCM). (C) Comparison of normalized average red fluorescence intensity present prior to photoconversion on a Nikon Eclipse Ti E SDCM or Olympus Fluoview FV1000 ($n = 10$).

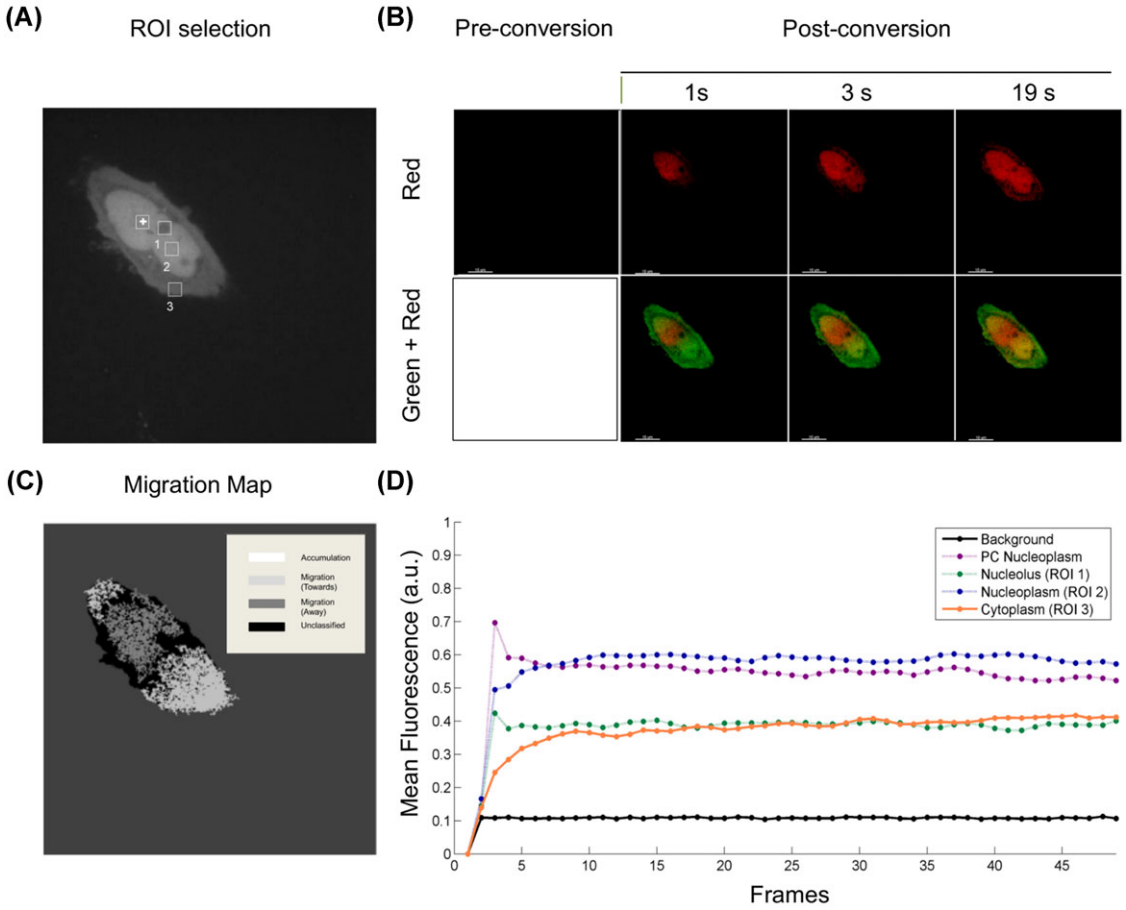

Fig. 3. Dendra2 freely diffuses between nucleoplasm and cytoplasm. (A) Dendra2 displays a diffuse localization within HeLa cells. (B) Snapshots of Dendra2 subcellular trafficking in HeLa cells. Dendra2 migration was tracked by acquiring a time series in the Red channel (one frame per s) for 45 frames. Green + Red: Red image series merged with the Green image obtained at the time of conversion. Bars, 10 μm. (C) Migration map of Dendra2 subcellular diffusion. (D) Analysis of Dendra2 diffusion through nucleolar (ROI1), nucleoplasmic (ROI 2) and cytoplasmic subcompartments (ROI 3).

Indeed, Fibrillarin accumulates in the Dense Fibrillar Centre of nuclei, where it participates in pre-rRNA processing and ribosome assembly (Hernandez-Verdun, 2006a). We targeted a region of nucleoplasm for PC (white cross) and monitored adjacent nuclear ROIs for Dendra2Fibrillarin relocalization using the red channel (Table 1; Figs 4A,D). For this analysis, two nucleoli were selected as ROIs in conjunction with a region in the nucleoplasm, located between the two nucleoli. As soon as 300 ms post-PC, Dendra2Fibrillarin was detected in the periphery of the nucleolus (ROI 1) closest to the PC region (Figs. 4A,D). Next, we could observe Fibrillarin migration through the intervening nucleoplasm (ROI 2) before accumulating in the second nucleolus (ROI 3; Figs. 4B,D). This was accompanied by concomitant decreased signal intensity in the PC region (Fig. 4D). Our observations are in agreement with previous studies describing the accumulation and dynamic association of Fibrillarin with the nucleolus (Phair RDM, 2000; Chudakov *et al.*, 2007b; Muro *et al.*, 2010). The migration map provides an integrated view of how Fibrillarin migrated throughout the entire nucleoplasm, but preferentially accumulated in the nucleoli (Fig. 4C).

Application 3: examining UBC9 subnuclear trafficking

Dendra2UBC9 localized to distinct subcellular compartments, including the cytoplasm, nucleus and PML protein nuclear bodies, which are the site of UBC9 accumulation, and corresponded to small bright and punctuated accumulation of higher fluorescence intensity. Indeed, UBC9 mediates the SUMOylation of PML proteins, which is crucial for PML nuclear body assembly (Duprez *et al.*, 1999; Wang *et al.*, 2004; Villagra *et al.*, 2006; Matera *et al.*, 2009; Jenne *et al.*, 2011). We delineated a region of nucleoplasm for PC (white cross) and monitored four adjacent ROIs for Dendra2UBC9 relocalization using the red channel (Table 1; Figs. 5A,D). These ROIs included two PML bodies, one nucleoplasmic and one

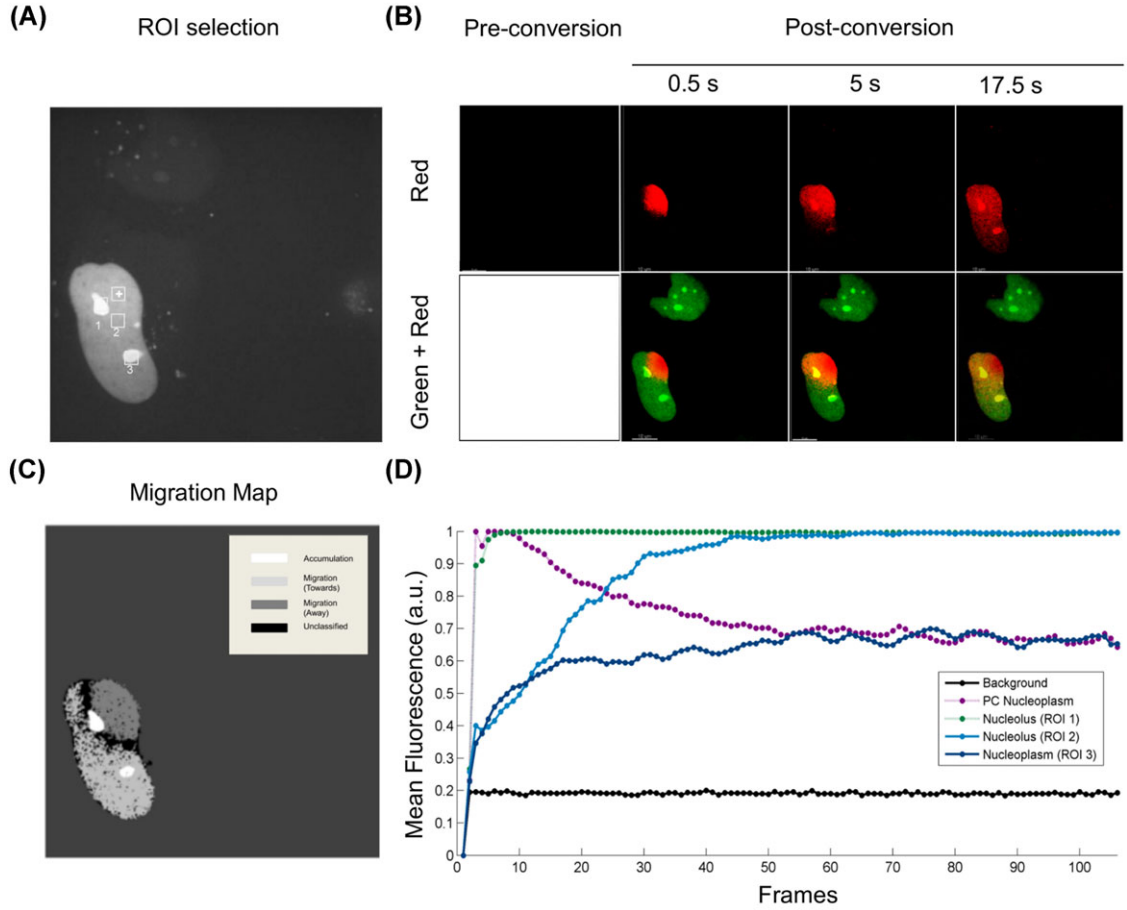

Fig. 4. Dendra2Fibrillarin trafficks between nucleoli via the nucleoplasm. (A) Dendra2Fibrillarin displays a nucleolar distribution in HeLa cells. (B) Snapshots of Dendra2Fibrillarin subnuclear trafficking. Dendra2Fibrillarin migration was tracked by acquiring a time series in the Red channel (one frame per 500 ms) for 120 frames. Green + Red: Red image series merged with the Green image obtained at the time of conversion. Bars, 10 μm. (C) Migration map of Dendra2Fibrillarin subnuclear trafficking. (D) Analysis of Dendra2Fibrillarin trafficking between two nucleoli (ROI 1 and ROI 2), via the nucleoplasm (PC, ROI 3).

cytoplasmic region (Fig. 5A). We observed the migration of the nucleoplasmic Dendra2UBC9 to the closest PML body (ROI 1) than to the adjacent nucleoplasm (ROI 2) before reaching the more distant PML body (ROI 3). In parallel, we observed a weak signal for Dendra2UBC9 in the cytoplasm, suggesting some level of Dendra2UBC9 nuclear export. The trafficking map underlines how Dendra2UBC9 protein moves through the nucleoplasm and interacts with PML bodies, where it accumulates (Fig. 5C).

Application 4: investigating the association of Dendra2UBC9 with PML bodies

As described above, Dendra2UBC9 displayed some apparent immobile fraction in the PML nuclear bodies. To examine whether the protein is transiently or permanently associated with PML bodies, we targeted one PML body for PC (white cross) and monitored two additional ROIs for Dendra2UBC9 relocalization using the red channel, including a nucleoplasmic region (ROI 1) and a more distant PML body (ROI 2; Table 1; Figs. 6A,D). Following PC, we observed the rapid decline in the PML body red fluorescent signal suggesting that Dendra2UBC9 is transiently associated with this nuclear body (Fig. 6D). This initially coincided with an increase in the nucleoplasm fluorescence (ROI 1) followed by the fluorescence accumulation in the second PML body (ROI 2). Interestingly, equilibrium was met between the two PML bodies, suggesting the shuttling of Dendra2UBC9 between the two PML bodies via the nucleoplasm.

Overall, we show here that Dendra2UBC9 is in constant flux and moves throughout the entire nucleus, regardless of its initial location. Indeed, we observed that Dendra2UBC9 is in constant exchange between the nucleoplasm and PML bodies, where it accumulates, and *vice et versa*. These results are in agreement with a leading model of UBC9 trafficking to the PML bodies and interacting and SUMO-modifying PML proteins (Villagra *et al.*, 2006).

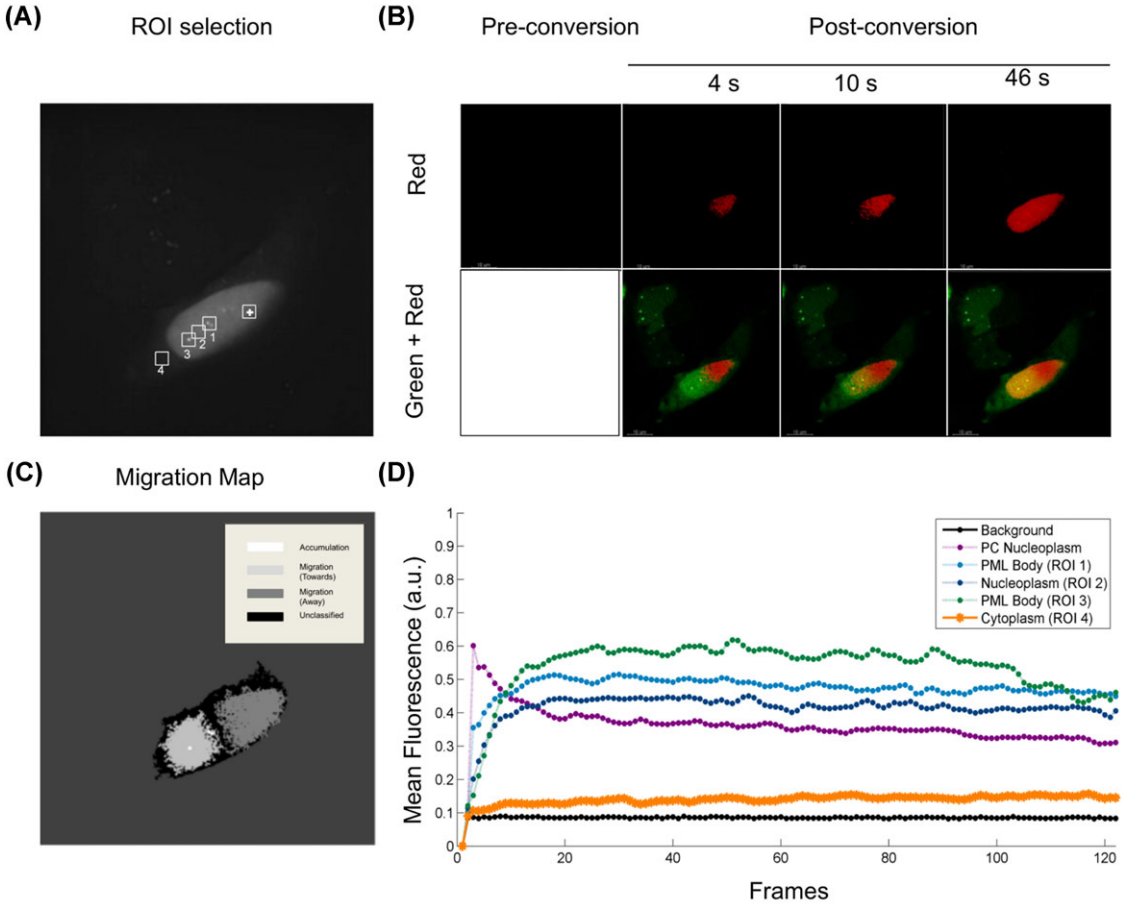

Fig. 5. Dendra2UBC9 trafficks between nuclear subcompartments. (A) Dendra2UBC9 is distributed between the nucleus and cytoplasm in HeLa cells. (B) Snapshots of Dendra2UBC9 subcellular trafficking. Dendra2UBC9 migration was tracked by acquiring a time series in the Red channel (one frame per s) for 120 frames. Green + Red: Red image series merged with the Green image obtained at the time of conversion. Bars, 10 μm. (C) Migration map of Dendra2UBC9 subnuclear trafficking. (D) Analysis of Dendra2UBC9 nucleoplasmic (PC, ROI 2) trafficking to PML bodies (ROI1 and ROI 3) and cytoplasm (ROI 4).

Next, we further examined the efficacy of the SDCM versus the LSCM in tracking rapid nuclear relocalization events, and employed the Olympus Fluoview FV1000 LSCM operated under fast scanning conditions (1 frame/1.6 s; 512 × 512 pixels; sampling speed 4 μs pixel^{-1}) to monitor Dendra2UBC9 inter-PML body trafficking (Fig. S2). Importantly, we observed that although the LSCM and the SDCM offer comparable resolution of UBC9 intra nuclear body trafficking, the SDCM still present the advantage to extensively reduce the premature PC during the image acquisition stage (Fig. 2C). Of note, although an exposure time of 50 ms was employed in this study to facilitate EMCCD synchronization at high disk speeds (5000 rpm), we anticipate that the additional capacity of the SDCM for shorter exposure image acquisition could potentially increase temporal resolution beyond that of the LSCM.

Conclusions

We present here an efficient and reproducible technique for the PC of Dendra2 tagged fusion proteins on a Nikon SDCM equipped with a FRAP-PA unit using nuclear proteins with contrasting dynamics as examples. Crucially, SDCM are preferentially employed for live cell imaging due to their high signal to noise ratio and the lower excitation energy necessary for fluorophore visualization. As such, our experimental approach is advantageous with respect to LSCM based techniques as it enables the analysis of protein trafficking *in vivo* while minimizing phototoxic effects which may induce alterations in protein trafficking at the subcellular level. Indeed, Dendra2 PC on the SDCM was reliably achieved with 1000 μs pixel^{-1} of irradiation with violet light (405 nm), whereas efficient PC on LSCM and epifluorescent microscopes require longer irradiation times with a correspondingly higher potential for phototoxicity (Chudakov *et al.*, 2007a; Baker *et al.*, 2010). Further-more, the high temporal resolution of this system enables capturing of rapid protein relocalization events, making it particularly suited to the study of fast trafficking proteins at the subnuclear level and in particular, their association with extremely small nuclear subcompartments (PML bodies).

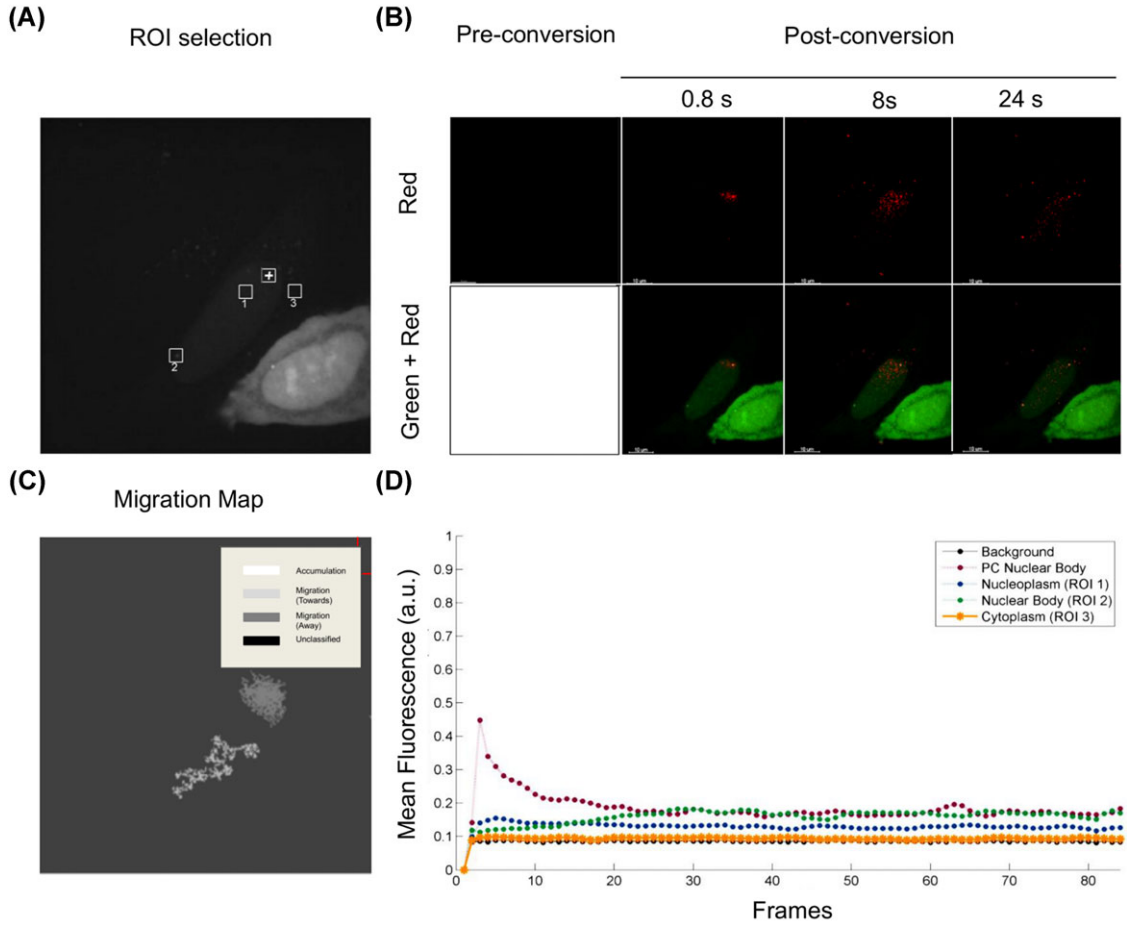

Fig. 6. Dendra2UBC9 is dynamically associated with PML nuclear bodies. (A) Dendra2UBC9 accumulates in subnuclear PML nuclear bodies in HeLa cells. (B) Snapshots of Dendra2UBC9 migration between PML bodies. Dendra2UBC9 migration was tracked by acquiring a time series in the Red channel (one frame per 800 ms) for 85 frames. Green + Red: Red image series merged with the Green image obtained at the time of conversion. Bars, 10 μm. (C) Migration Map of Dendra2UBC9 trafficking between PML bodies. (D) Analysis of Dendra2UBC9 shuttling between PML bodies (PC, ROI 2) via the nucleoplasm (ROI 1) and cytoplasm (ROI 4).

Materials and methods

Plasmids

Dendra2-C and Dendra2Fibrillarin expression vectors were a generous gift from Dr. Konstantin Lukyanov (Institute of Bioorganic Chemistry, Russian Academy of Sciences, Moscow, Russia; Chudakov *et al.*, 2007b). Dendra2UBC9 was obtained by PCR amplification of the cDNA encoding UBC9 from pCDNA3-UBC9-SV5, obtained from Dr. Ronald Hay (University of St. Andrews, St. Andrews, UK) and cloning in frame into the *EcoR1* sites of the Dendra2-C expression vector.

Cell culture

HeLa cells (ATCC CCL-2) were maintained in Dulbecco's Modified Eagles Medium supplemented with 10% foetal calf serum at 37°C in a humidified atmosphere of 5% CO_2. 24 h before imaging, HeLa cells grown in μ-slides (IBIDI) were transfected with 50 ng of Dendra2, Dendra2Fibrillarin or Dendra2UBC9 complexed with 0.15 μl Fugene HD (Roche Applied Science, Manheim, Germany). Prior to PC experiments, Dulbecco's Modified Eagles Medium was exchanged for HEPES buffered Dulbecco's Modified Eagles Medium without phenol red supplemented with 10% foetal calf serum.

PC experiments

SDCM. PC experiments were performed on a SDCM which consisted of a confocal spinning disk unit X1 (Yokagawa Electric Corporation, Tokyo, Japan) mounted on a Nikon Eclipse Ti E inverted microscope, and equipped with a Plan-Apochromat VC 100×/1.4 N.A. oil objective (Nikon) and 100 mW 405

nm, 50 mW 488 nm diode and 50 mW 561 nm diode pumped solid stareDPSS laser lines. Cells were maintained at 37°C in a humidified atmosphere (5% CO_2) for the duration of the experiment. The Dendra2 signal (Green) was excited with a 488 nm laser at 1–8.5% laser power, and emission was detected at 512/18 nm. A subcellular region was targeted using a FRAP-PA unit (Andor) and photoconverted with a short pulse (1000 μs pixel^{-1}) of a 405 nm diode laser administered at 25% laser power. Photoconverted Dendra2 (Red) signal was excited with a 561 nm diode pumped solid stare laser at 25% laser power and emission detected at 624/40 nm. Dendra2 trafficking events were monitored by capturing Dendra2 (Red) signal over time using an iXon 897 EMCCD (Andor) camera (air cooled to −70°C) in conjunction with Andor IQ2 acquisition software.

LSCM. PC experiments were carried out on an Olympus Fluoview FV1000 microscope equipped with a 60× objective and 50 mW 405 nm diode, 488 nm diode and 559 nm diode pumped solid stare nm laser lines. Cells were maintained at 37°C in a humidified atmosphere (5% CO_2) for the duration of the experiment. The Dendra2 signal (Green) was excited with a 488 nm laser (0.1%) and emission was detected using a GFP filter set. The Dendra2 signal (Red) was excited at 559 nm (14%) and detected using an RFP filter set. A control image in the Green and Red channels was recorded prior to PC to ensure no nonspecific PC events had occurred. Next, a subcellular region was targeted and photoconverted by applying of a short pulse (20 μs per pixel) of a 405 nm diode laser administered in tornado mode at 25% laser power. A time series was recorded in the red channel to monitor protein trafficking events using the following settings: (SIM scanner; 1 frame/1.6 s; 512 × 512 pixels; sampling speed 4 μs per pixel) and detected using a PhotoMultiplier Tube.

Photostability experiments

Photostability experiments were carried out on a Nikon Eclipse Ti E Spinning Disk (acquisition parameters as previously described). Cells were maintained at 37°C using a stage heater for the duration of the experiments. PC was achieved using a short pulse (1000 μs pixel^{-1}) of a 405 nm diode laser administered at 25% laser power. Dendra2 photostability was examined pre- and post-PC by acquiring 120 frames (pre-PC) or 86 frames (post-PC) sequentially in both Green and Red channels. The mean cell fluorescence intensity was normalized against the background signal and analysed over time with Andor IQ2.

Preconversion experiments

SDCM. Preconversion experiments were carried out on a Nikon Eclipse Ti E Spinning Disk (acquisition parameters as previously described). HeLa Cells expressing either Dendra2UBC9 or Dendra2Fibrillarin were maintained at 37°C using a stage heater for the duration of the experiments.

LSCM. Preconversion experiments were carried out on an Olympus Fluoview FV1000 (acquisition parameters as previously described). HeLa Cells expressing either Dendra2UBC9 or Dendra2Fibrillarin were maintained at 37°C using a stage heater for the duration of the experiments.

Analysis. Preconversion was analysed by quantifying the average red-fluorescence intensity in the red channel, recorded prior to PC. A cellular ROI representing the cell nucleus was defined after PC and applied to the preconversion image. The average fluorescence intensity of the ROI was quantified and normalized against the background using Imagej (NIH). Graphs represent the average red fluorescence intensity in 10 independent experiments.

Image analysis

Analysis of photoconvertible protein trafficking was performed using MATtrack (available from http://eleceng.dit.ie/courtney/index.php?uid=417&menu_id=74), which was implemented in MATLAB, ver. 7.1. Spatial and temporal noise was removed by applying a 3 × 3 median and Gaussian filter, respectively. Next, the relative fluorescence intensity in the cellular compartment was normalized by subtracting the background signal, which was defined as the average red fluorescence intensity quantified from the entire control image recorded in the red channel prior to PC. Subsequently, a statistical model of the data set was built by calculating the average intensity (mean) and SD of each pixel in the data set. ROI selection was performed on the Mean image of the data set by manually identifying a structure of interest and employing a seeded region growing algorithm (Tanaami *et al.*, 2002) to automatically seek out adjacent pixels of equivalent mean intensity (up to 50) for inclusion in the ROI. Finally, the fluorescent signal in the ROI was quantified over the time series and plotted (Mean Fluorescence against Frame no.) to characterize the trafficking of Dendra2 fusion proteins.

Conflicts of interest

The author(s) declare that they have no competing interests.

Author's contributions

EW performed the PC experiments and drafted the manuscript. JC designed the analytical software used in this publication. VWG conceived and designed the experiments and drafted the manuscript. DS provided technical expertise on the operation of the SDCM, subsequent experimental design.

Acknowledgements

This work was supported by the UCD National Virus Reference Laboratory (NVRL). The authors wish to acknowledge access to and use of the UCD Conway Imaging Core Technologies, Conway Institute for Biomolecular and Biomedical Research, University College Dublin. In particular, we wish to acknowledge Prof. Dimitri Scholz director of Biological Imaging, Conway institute, UCD, and Katarzyna Welzel for their assistance with image acquisition and PC on the SDCM, the latter being funded by Science Foundation Ireland (SFI). Finally, the authors wish to acknowledge Dr. Konstantin Lukyanov for his extremely generous gifts of the Dendra2c and Dendra2Fibrillarin vectors (Institute of Bioorganic Chemistry, Russian Academy of Sciences, Moscow, Russia).

References

Adam, V., Nienhaus, K., Bourgeois, D. & Nienhaus, G.U. (2009) Structural basis of enhanced photoconversion yield in green fluorescent protein-like protein Dendra2. *Biochemistry* **48**, 4905–4915.

Adams, R. & Bischof, L., (1994) Seeded region growing. *IEEE. Trans. PAMI.* **16**, 641–647.

Baker, S.M., Buckheit, R.W. & Falk, M.M. (2010) Green-to-red photoconvertible fluorescent proteins: tracking cell and protein dynamics on standard wide-field mercury arc-based microscopes. *BMC. Cell. Biol.* **11**, 15.

Chudakov, D.M., Chepurnykh, T.V., Belousov, V.V., Lukyanov, S. & Lukyanov, K.A. (2006) Fast and precise protein tracking using repeated reversible photoactivation. *Traffic* **7**, 1304–1310.

Chudakov, D.M., Lukyanov, S. & Lukyanov, K.A. (2007a) Tracking intracellular protein movements using photoswitchable fluorescent proteins PS-CFP2 and Dendra2. *Nat. Protoc.* **2**, 2024–2032.

Chudakov, D.M., Lukyanov, S. & Lukyanov, K.A. (2007b) Using photoactivatable fluorescent protein Dendra2 to track protein movement. *Biotechniques* **42**, 553–563.

Duprez, E., Saurin, A.J., Desterro, J.M., *et al.* (1999) SUMO-1 modification of the acute promyelocytic leukaemia protein PML: implications for nuclear localisation. *J. Cell. Sci.* **112**, 381–393.

Enoki, R., Ono, D., Hasan, M.T., Honma, S. & Honma, K. (2012) Single-cell resolution fluorescence imaging of circadian rhythms detected with a Nipkow spinning disk confocal system. *J. Neurosci. Methods* **207**: 72–79.

Földes-Papp, Z., Demel, U & Tilz, G.P. (2003) Laser scanning confocal fluorescence microscopy: an overview. *Int. Immunopharmacol.* **3**, 1715–1729.

Genka, C., Ishida, H., Ichimori, K., Hirota, Y., Tanaami, T. & Nakazawa, H. (1999) Visualization of biphasic Ca2+diffusion from cytosol to nucleus in contracting adult rat cardiac myocytes with an ultra-fast confocal imaging system. *Cell Calcium.* **25**, 199–208.

Gurskaya, N.G., Verkhusha, V.V., Shcheglov, A.S., Staroverov, D.B., Chepurnykh, T.V., Fradkov, A.F., Lukyanov, S. & Lukyanov, K.A. (2006) Engineering of a monomeric green-to-red photoactivatable fluorescent protein induced by blue light. *Nat. Biotechnol.* **24**, 461–465.

Hernandez-Verdun, D. (2006a) The nucleolus: a model for the organization of nuclear functions. *Histochem. Cell. Biol.* **126**, 135–148.

Hernandez-Verdun, D. (2006b) Nucleolus: from structure to dynamics. *Histochem. Cell. Biol.* **125**, 127–137.

Inoué, S. & Inoué, T. (2002) Chapter 2, Direct-view high-speed confocal scanner: the CSU-10. Methods in Cell Biology (ed. by M. Brian), pp. 87–127. Academic Press.

Jenne, C.N., Wong, C.H.Y., Petri, B. & Kubes, P. (2011) The use of spinning-disk confocal microscopy for the intravital analysis of platelet dynamics in response to systemic and local inflammation. *PLoS. One*. **6**, 1–13.

Kuzmenko, A., Tankov, S., English, B.P., Tarassov, I., Tenson, T., *et al.* (2011) Single molecule tracking fluorescence microscopy in mitochondria reveals highly dynamic but confined movement of Tom40. *Sci. Rep.* **1**, 195.

Lam, P.Y., Fischer, R.S., Shin, W.D., Waterman, C.M. & Huttenlocher, A. (2014) Spinning disk confocal imaging of neutrophil migration in zebrafish. *Methods Mol. Biol.* **1124**, 219–233.

Lukyanov, K.A., Chudakov, D.M., Lukyanov, S. & Verkhusha, V.V. (2005) Innovation: photoactivatable fluorescent proteins. *Nat. Rev. Mol. Cell. Biol.* **6**, 885–891.

Matera, A.G., Izaguire-Sierra, M., Praveen, K. & Rajendra, T.K. (2009) Nuclear bodies: random aggregates of sticky proteins or crucibles of macromolecular assembly? *Dev. Cell.* **17**, 639–647.

Mayer, C. & Grummt, I. (2005) Cellular stress and nucleolar function. *Cell Cycle* **4**, 1036–1038.

Mueller, F., Mazza, D., Stasevich, T.J. & McNally, J.G. (2010) FRAP and kinetic modeling in the analysis of nuclear protein dynamics: what do we really know? *Curr. Opin. Cell. Biol.* **22**, 403–411.

Muro, E., Gébrane-Younès, J., Jobart-Malfait, A., Louvet, E., Roussel, P. & Hernandez-Verdun, D. (2010) The traffic of proteins between nucleolar organizer regions and prenucleolar bodies governs the assembly of the nucleolus at exit of mitosis. *Nucleus* **1**, 202–211.

Nakano, A. (2002) Spinning-disk confocal microscopy; a cutting-edge tool for imaging of membrane traffic. *Cell Struct. Func.* **27**, 349–355.

Nelson, M., Ledoux, J., Taylor, M., *et al.*, (2010) Spinning disk confocal microscopy of calcium signalling in blood vessel walls. *Microsc. Anal. (Am Ed)*. **1**, 5–8.

Olson, M.O. & Dundr, M. (2005) The moving parts of the nucleolus. *Histochem. Cell. Biol.* **123**, 203–216.

Phair RDM, T. (2000) High mobility of proteins in the mammalian cell nucleus. *Nature* **404**, 604–609.

Samantha Stehbens, H.P., Lindsay, Murrow & Torsten, Wittmann. (2012) Imaging intracellular protein dynamics by spinning disk confocal microscopy. *Methods Enzymol* **504**, 293–313.

Scheer, U. & Hock, R. (1999) Structure and function of the nucleolus. *Curr. Opin. Cell. Biol.* **11**, 385–390.

Sprague, B.L. & McNally, J.G. (2005) FRAP analysis of binding: proper and fitting. *Trends Cell. Biol.* **15**, 84–91.

Tanaami, T., Otsuki, S., Tomosada, N., Kosugi, Y., Shimizu, M. & Ishida, H. (2002) High-speed 1-frame/ms scanning confocal microscope with a microlens and nipkow disks. *Appl. Opt.* **41**, 4704–4708.

Villagra, N., Navascues, J., Casafont, I., Val-Bernal, J. F., Lafarga, M. & Berciano, M. (2006) The PML-nuclear inclusion of human supraoptic neurons: a new compartment with SUMO-1 - and ubiquitin–proteasome-associated domains. *Neurobiol. Dis.* **21**.

Wang, E., Babbey, C.M. & Dunn, K.W. (2005) Performance comparison between the high-speed Yokogawa spinning disc confocal system and single-point scanning confocal systems. *J. Microsc.* **218**, 148–159.

Wang, J., Shiels, C., Sasieni, P., Wu, P.J., Islam, S.A., *et al.* (2004) Promyelocytic leukemia nuclear bodies associate with transcriptionally active genomic regions. *J. Cell. Biol.* **164**, 515–526.

White, J.G., Amos, W.B. & Fordham, M. (1987) An evaluation of confocal versus conventional imaging of biological structures by fluorescence light microscopy. *J. Cell. Biol.* **105**, 41–48.

